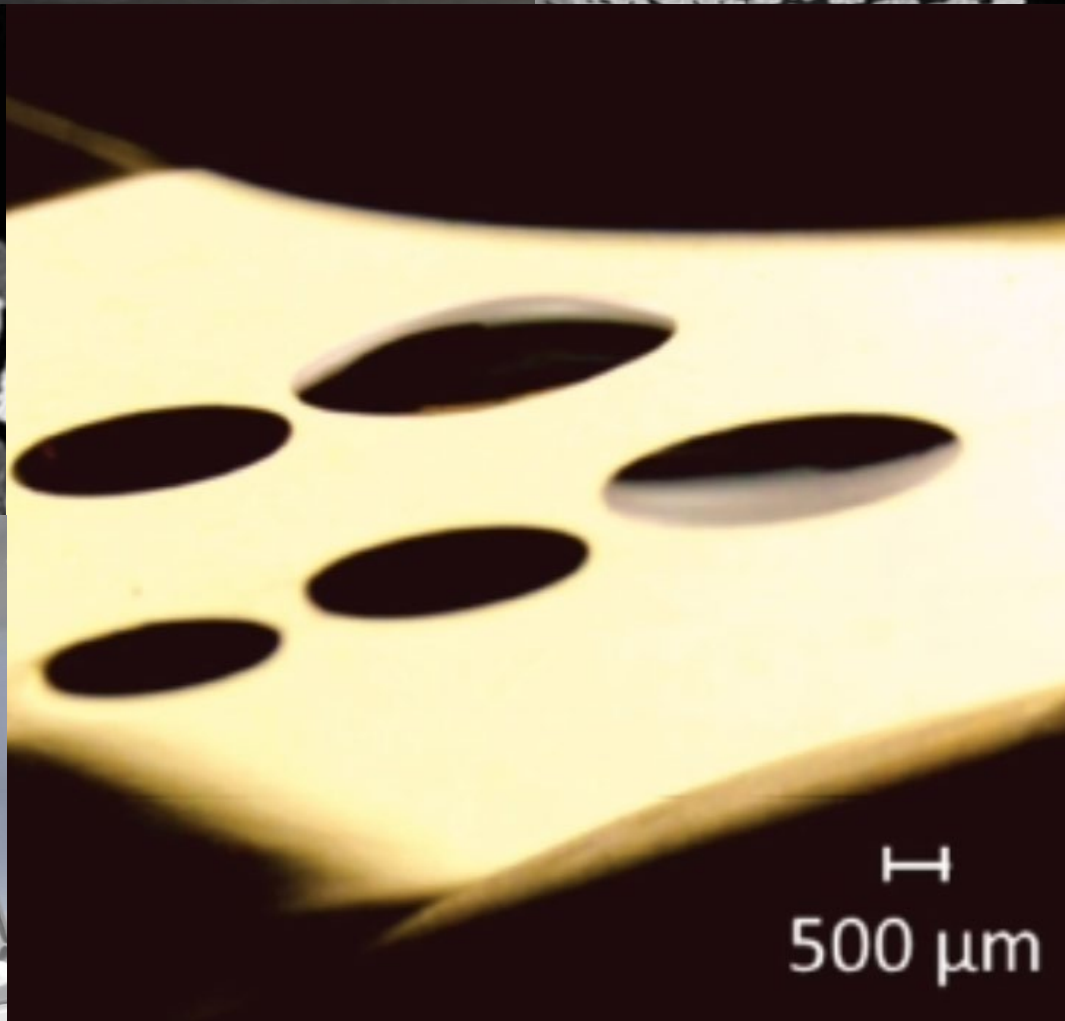
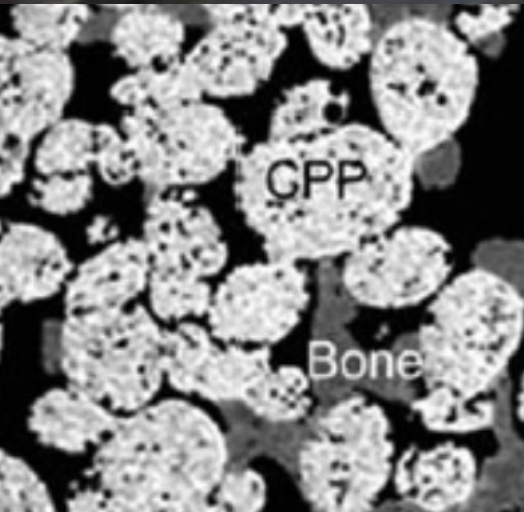
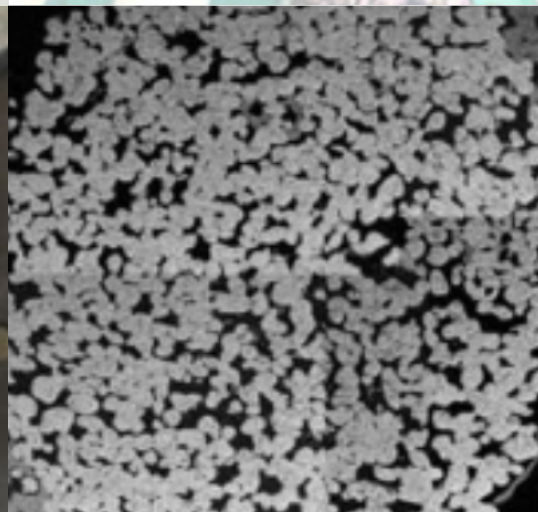
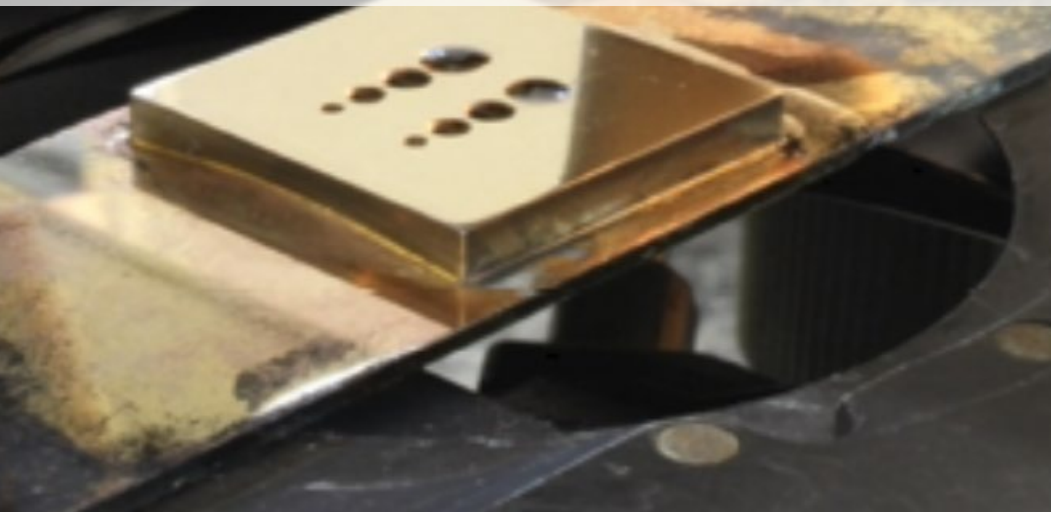


Gravimetric Analysis: Determining the Density of a Sample for Various Applications

Expert Insights



SARTORIUS

Wiley Analytical Science

Contents

- 3** Editorial
- 4** Introduction
- 6** Error calculations
- 10** Bulk density measurements of small solid objects using laser confocal microscopy
- 14** Solid freeform fabrication of porous calcium polyphosphate structures for bone substitute applications: In vivo studies

Editorial

Dear Readers,

Determining the density of a sample is one of the most frequently used gravimetric methods in laboratories. Changes in density can indicate that the product or material in question no longer has the specified properties. When combined with other data, it is possible to gain insight into the possible cause of the change in quality.

Accurate determination of the density of a given sample has been a challenge since the time of ancient Greece. The measurement protocol discovered by Archimedes is still applied today, although in containers smaller than a bathtub. Nowadays, the challenges have shifted from determining crown compositions to various applications, ranging from medicinal research to materials science applications.

This book will take you from the basics of mass determination to how to mathematically assess errors that are inherent to every measurement.

The book concludes with two recent applications of Sartorius weighing equipment in scientific research.

Best,

Dr. Martin Graf-Utzmann

Editor at Wiley Analytical Science

Introduction

Measuring the density of an object without manipulating its shape dates back to the Greek scholar Archimedes (287–212 B.C.). As a quality control for gold content, Archimedes immersed a crown in water and compared the displaced liquid volume with that of a reference sample to calculate and compare the measured densities. His technique was based on the following physics principle. The buoyancy of a sample is directly proportional to the displaced volume. Thus, the higher density samples proportionally displace lower volumes of the liquid as reflected in the formula:

$$F_{\text{buoyancy}} = V_{\text{displaced}} \times \rho_{\text{Fluid}} \times g.$$

F_{buoyancy} is the buoyancy force, $V_{\text{displaced}}$ is the amount of volume displaced by the solid, ρ_{fluid} is the density of the fluid, and g is the gravitational acceleration.

The Iranian polymath scholar Abu Raihan Muhammad al-Biruni (973–1048 A.D.) constructed the first pycnometer to measure the density of various elements. The pycnometer, a glass vessel with a defined volume, uses liquid displacement as the underlying principle. The measurement process begins with weighing the empty vessel or the vessel filled with water. The test liquid or solid is added to the vessel, and the measured difference in weight is used to calculate the density of the test liquid or solid.

Additional density measurement devices were developed in the 18th century. Popular inventions included scaled glass measuring devices such as aerometers. These devices also operate on the original Archimedes principle. Aerometers are still used today for select applications such as the determination of alcohol concentration.

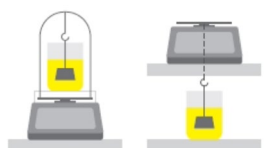
Today, quality control (QC) of raw products, intermediates, and finished products often relies on their density measurements as a major characteristic. While QC uses the same underlying principles for measuring density, modern laboratories benefit from advanced instruments with guided protocols that simplify the process of performing density measurements by the standard methods:

- Buoyancy method
- Displacement method
- Pycnometers

Recordkeeping is an important component of today's regulated environment and has become more time-consuming over the years. Advanced instruments use integrated electronic data processing to digitally log ambient conditions and the measured weight values. The density is calculated automatically. After completing the program task(s), the advanced instrument sends a report to the user with all recorded data and the calculated results. These features enhance data reliability in the laboratory by minimizing errors in measurements and recordkeeping.

Comparison of Methods for Density Determination

Characteristic	Buoyancy method	Displacement method	Pycnometer
Suitable for	<ul style="list-style-type: none"> • Solid state • Liquids • Dispersions • Gases 	<ul style="list-style-type: none"> • Solid state • Liquids • Dispersions 	<ul style="list-style-type: none"> • Solid state powders, granuals • Liquids • Dispersions
Advantages	Suitable for almost all sample types	Suitable for almost all sample types	Suitable for almost all sample types
	Flexible with sample size	Flexible with sample size	
	Rapid process	Rapid process	Very accurate
	Balances with integrated software, operator guidance, and evaluation are already available	Balances with integrated software, operator guidance, and evaluation are already available	Balances with integrated software, operator guidance, and evaluation are already available
	Easy test evaluation	Easy test evaluation	Easy test evaluation
Disadvantages	Tempering of liquids and solid-state bodies requires work	Tempering of liquids and solid-state bodies requires work	Tempering of liquids and solid-state bodies requires work
	Liquid density determination requires large sample volume	Liquid density determination requires large sample volume	Liquid density determination is labor-intensive
		Liquid evaporation can affect results	Time-intensive
	Thorough wetting of sample required	Thorough wetting of sample required	
	Air bubbles must be avoided or removed	Air bubbles must be avoided or removed	Air bubbles must be avoided or removed
Measurement uncertainty	Dependent on balance, sample quantity, and/or sample density	Dependent on balance, sample quantity, and/or sample density	Dependent on balance, sample quantity
Readability 1 mg	Solids: <0.4% for 10g sample Liquids: <0.20% for sample $\rho = 1.3 \text{ g/cm}^3$	Solids: <0.2% for sample >50g (in water), $\rho = 5 \text{ g/cm}^3$.	<0.2% for sample >20g
Readability 0.1 mg	Solids: <0.1% for samples >5g Liquids: <0.11% for sample $\rho = 1.8 \text{ g/cm}^3$	Solids: <0.2% for sample >50g (in water), $\rho = 5 \text{ g/cm}^3$.	< 0.003% for sample > 10g
Readability 0.01 mg	Solids: <0.10% for samples >5g (in water) <0.15% for samples >5g (in ethanol) Liquids: <0.1% for sample $\rho < 1.5 \text{ g/cm}^3$	< 0.005% for sample > 10g	



The beaker with liquid stands on a platform or below the scale

Buoyancy method



The beaker with liquid is on the scale

Displacement method



Glass vessel with defined volume

Pycnometer

Content adapted from Weighing Application Compendium: Density Determination (Sartorius).

Error calculations

Pycnometer method

The errors in density determination can be kept as low as possible by paying particular attention to the following aspects of the procedure:

- Constant temperature (variation <0.1°C) is essential during procedure:
 - A change of 0.1°C in the auxiliary liquid water causes a density change of 0.00002 to 0.0003 g/cm³.
 - When the auxiliary liquid is alcohol, density changes approx. 0.0001 g/cm³.
- No air bubbles in auxiliary liquid or sample.
- Air buoyancy causes an error in the density of approx. 0.0012 g/cm³.

With precise adherence to procedure, the pycnometer can be used to determine material densities very accurately.

Error calculations

Performing each step of the procedures thoroughly and avoiding the systemic errors mentioned above, the error of density determination can be calculated according to the rules of error propagation. The error of the density $\Delta\rho$ is mainly based on the errors of measurement of mass. As a general rule, the total error ΔF is calculated from several measured values:

For errors expressed as sums (or differences), the absolute single errors add up quadratically:

$$F = \Delta F_1^2 + F_2^2 + \dots$$

where ΔF is total error, and ΔF_n is an absolute single error expressed as a sum where n is an integer and represents each measured value.

For errors expressed as products (and quotients), the relative single errors (ΔF_x) add up quadratically. The relative error is the absolute error related to the measured value.

$$\Delta F = \sqrt{\left[\frac{\Delta F_1}{F_1}\right]^2 + \left[\frac{\Delta F_2}{F_2}\right]^2} + \dots$$

Buoyancy method

The determination of the density of solids by the buoyancy method applies the following relation:

$$\rho_s = \rho_{fl} \times \frac{m_{(a)}}{\Delta m_{(a)} - m_{(fl)}}$$

or

$$\rho_s = (\rho_{fl} - \rho_a) \times \frac{W_{(a)}}{[W_{(a)} - W_{(fl)}] \times \text{Corr}} + \rho_a$$

where ρ_s is density of solid, ρ_{fl} is density measured in fluid, ρ_a is density measured in air, $m_{(a)}$ is the mass measured in air, $m_{(fl)}$ is the mass measured in fluid, $W_{(a)}$ is weight value in air, and $W_{(fl)}$ is the weight value measured in the fluid. Since the correction factors for the density of the air and the sample holder do not influence the error of the density calculation, they do not need to be considered in the calculation of the error.

Basic rules of error calculation

First, the absolute error of the denominator, $\Delta[m_{(a)} - m_{(fl)}]$ is calculated where $m_{(a)}$ is the mass measured in air and $m_{(fl)}$ is the mass measured in fluid.

$$\Delta[m_{(a)} - m_{(fl)}] = \sqrt{\Delta m_{(a)}^2 + m_{(fl)}^2}$$

The total relative density error, $\Delta\rho/\rho$ is calculated with

$$\frac{\Delta\rho}{\rho} = \sqrt{\left[\frac{\Delta\rho_{fl}}{\rho_{fl}}\right]^2 + \left[\frac{\Delta m_{(a)}}{m_{(a)}}\right]^2 + \left[\frac{\Delta m_{(a)} - m_{(fl)}}{m_{(fl)}}\right]^2}$$

where $\Delta\rho$ is error in density, ρ is density of material, $\Delta\rho_{fl}$ is error in density measured in fluid, $m_{(a)}$ is the mass measured in air, $\Delta m_{(a)}$ is total error of weighing in air, $m_{(a)}$ is mass measured in air, and $m_{(fl)}$ is the mass measured in fluid. The total error of weighing in air $\Delta m_{(a)}$ is independent of balance type, because it involves differential weighing. The total error of weighing in air $\Delta m_{(a)}$ is the sum of the linearity error of one digit and the reproducibility error.

The maximum error for weighing in liquid $\Delta[m_{(a)} - m_{(fl)}]$ is assumed to be on average 10 times larger than weighing in air. This assumption is based on numerous measurements for density determination using the buoyancy method.

Liquid density error

A misreading of the thermometer by $\pm 0.1^\circ\text{C}$ or a temperature change of $\pm 0.1^\circ\text{C}$ during the measurement induces an error in the density of 0.00003 g/m³ of the material measured in water and 0.00009 g/m³ for the sample measured in ethanol.

The relative error of the solid density can be influenced by sample size and density as well as the buoyancy medium (water and ethanol). The error of the density determination is dependent on the sample density: the lower the density of the sample, the greater the error of the final result (Fig. 1-6).

When calculating relative error of the solid density $\Delta\rho/\rho$

$$m_{(fl)} = m_{(a)} \times \left[1 - \frac{\rho_{fl}}{\rho_s} \right]$$

$\Delta\rho/\rho$ is used for $m_{(fl)}$. For ρ_{fl} the density of water is assumed to be 1.0 g/cm³, and the ethanol density is assumed to be 0.789 g/cm³.

Figures 1 – 6 show examples of the relative error of solid density determined by using Sartorius balances with different readabilities and ranges for the buoyancy method. Figures 1 – 3 show examples with the immersion fluid as water whereas Figures 4 – 6 show examples with the immersion fluid as ethanol.

Figure 1 shows the results from an immersion body with a volume of 10 + 0.01 cm³, a density of 2.48 g/cm³, and a tolerance of 0.5 mg related to buoyancy in water.

Displacement procedure

Determination of the solid density by the displacement method shows the following relation. The air density, ρ_a , is assumed to be constant and thus is not included in the calculation of the error.

$$\rho_s = \rho_{fl} \times \frac{m_s}{m_{fl}} = (\rho_s - \rho_{fl}) \times \frac{W_s}{W_{fl}} + \rho_a$$

$$\frac{\Delta\rho}{\rho} = \sqrt{\left[\frac{\Delta\rho_{fl}}{\rho_{fl}} \right]^2 + \left[\frac{\Delta m_{(a)}}{m_{(a)}} \right]^2 + \left[\frac{\Delta m_{(a)} - m_{(fl)}}{m_{(fl)}} \right]^2}$$

with

$$*m_{(fl)} = \frac{\rho_{fl}}{\rho_s} \times m_{(a)}$$

where ρ_s is density of solid, ρ_{fl} is density measured in fluid, ρ_a is density measured in air, $\Delta\rho$ is error in density, $m_{(a)}$ is the mass measured in air, $m_{(fl)}$ is the mass measured in the fluid, m_s is mass of the solid, $W_{(s)}$ is weight value of solid, and $W_{(fl)}$ is the weight value measured in the fluid.

Comparison of relative errors between solid density determination by buoyancy method and by displacement method

The results of the solid density determination with the buoyancy method (Fig. 1–6) show smaller

errors than those with the displacement method (Fig. 8). In the buoyancy method, the relative error decreases with increasing sample density. In contrast, the relative error of density determination by the displacement method increases with increasing sample density.

Pycnometer method

Density determination by the pycnometer method involves the following relation:

$$\rho_s = \rho_{fl} \times \frac{m_1}{m_1 + m_2 - m_3}$$

or

$$\rho_s = (\rho_{fl} - \rho_a) \times \frac{W_2}{W_1 + W_2 - W_3} + \rho_a$$

The air density error is neglected. The total error of the weight value is the sum of the reproducibility of the weighing type and a linearity error of one digit. The error of the liquid density determination is often assumed to be due to a change of temperature of $\pm 0.1^\circ\text{C}$ temperature during the procedure: the error value is 0.00003 g/cm³. As the auxiliary liquid, water has a density of 1.0 g/cm³.

First the error of the denominator $\Delta[m^1 + m^2 - m^3]$ is calculated

$$\Delta[m_1 + m_2 - m_3] = \sqrt{\Delta m_1^2 + \Delta m_2^2 + \Delta m_3^2}$$

(where m_n is the mass and n is an integer and represents each measured value) and then the total relative density error $\Delta\rho/\rho$

$$\frac{\Delta\rho}{\rho} = \sqrt{\left[\frac{\Delta\rho_{fl}}{\rho_{fl}} \right]^2 + \left[\frac{\Delta m_2}{m_2} \right]^2 + \left[\frac{\Delta(m_1 + m_2 - m_3)}{(m_1 + m_2 - m_3)} \right]^2}$$

where $\Delta\rho/\rho$ is the total relative density error, $\Delta\rho/\rho$ is the total relative density error, and Δm_n is the error of weighing mass and represents each measured value.

Figure 1

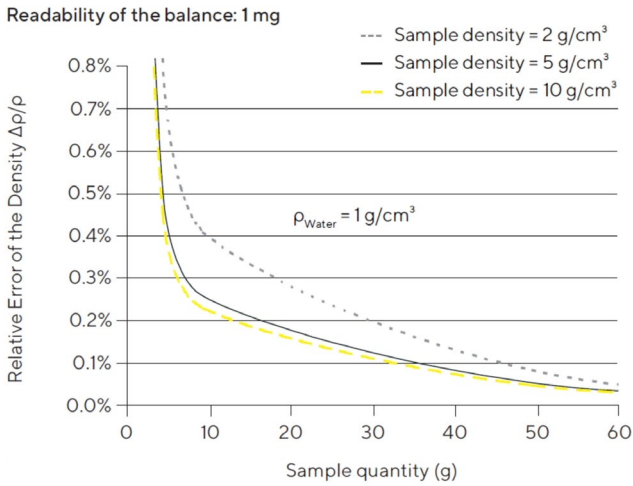


Fig. 1: Relative density error during solid density determination by the buoyancy method. Relative density error is dependent on sample size and sample density. Readability of the balance is 1 mg. Immersion fluid is water.

Figure 2

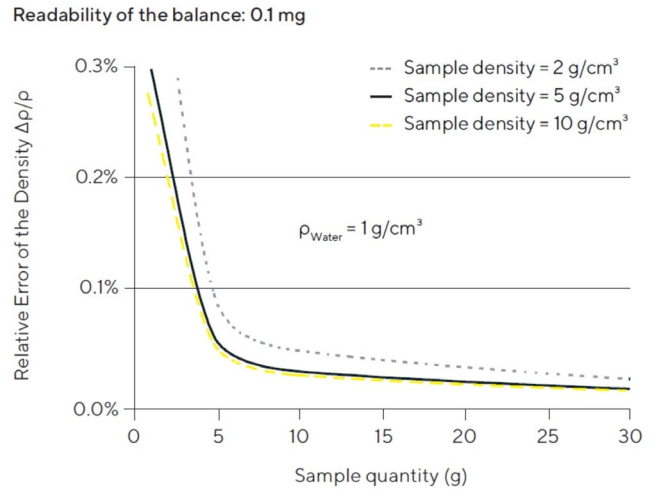


Fig. 2: Relative density error during solid density determination by the buoyancy method. Relative density error is dependent on sample size and sample density. Readability of the balance is 0.1 mg. Immersion fluid is water.

Figure 3

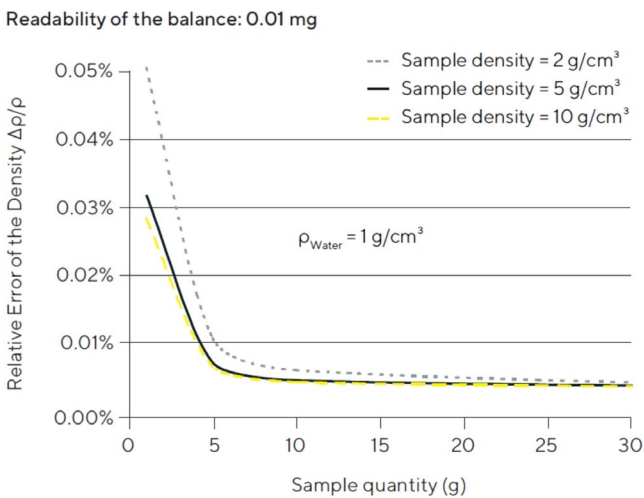


Fig. 3: Relative density error during solid density determination by the buoyancy method. Relative density error is dependent on sample size and sample density. Readability of the balance is 0.01 mg. Immersion fluid is water.

Figure 4

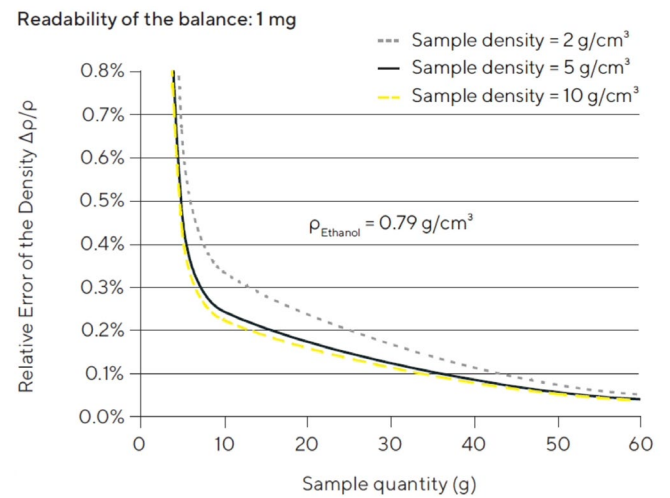


Fig. 4: Relative density error during solid density determination by the buoyancy method. Relative density error is dependent on sample size and sample density. Readability of the balance is 1 mg. Immersion fluid is ethanol.

Figure 5

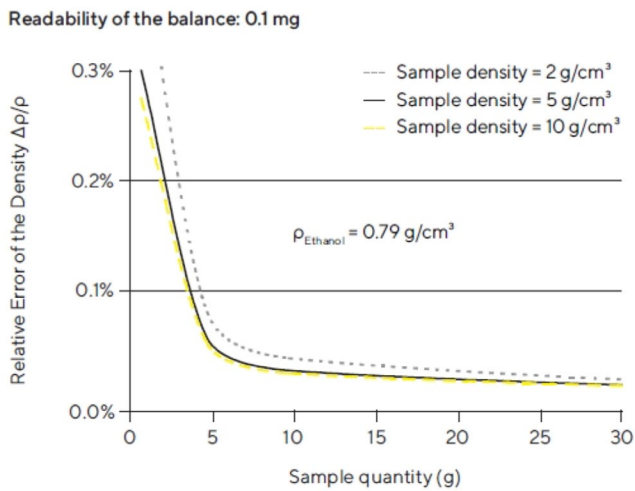


Fig. 5: Relative density error during solid density determination by the buoyancy method. Relative density error is dependent on sample size and sample density. Readability of the balance is 0.1 mg. Immersion fluid is ethanol.

Figure 6

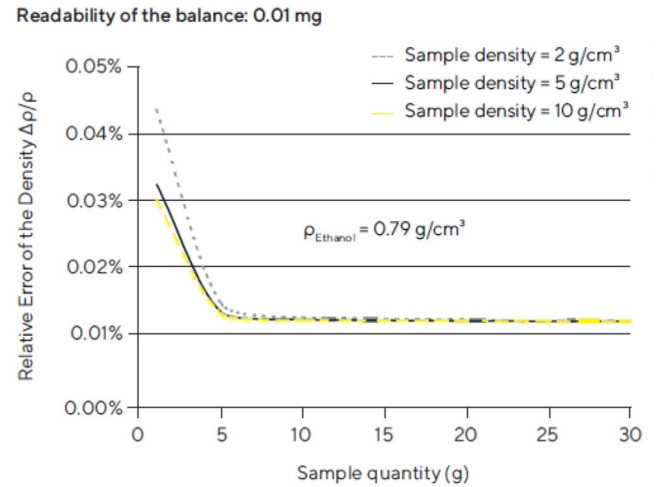


Fig. 6: Relative density error during solid density determination by the buoyancy method. Relative density error is dependent on sample size and sample density. Readability of the balance is 0.01 mg. Immersion fluid is ethanol.

Figure 7

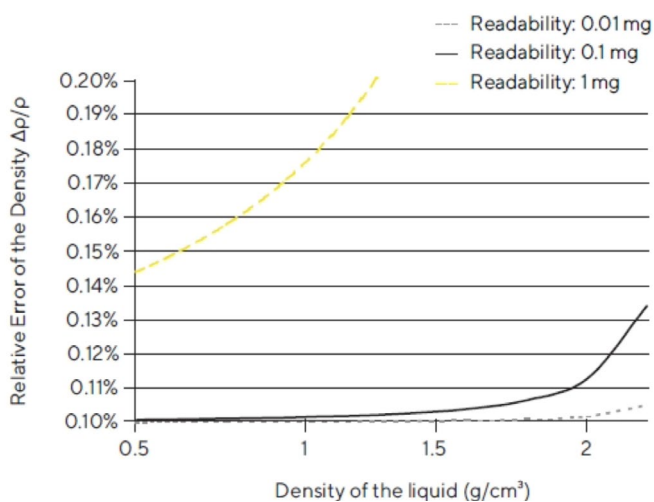


Fig. 7: Relative error of the density during liquid density determination by the buoyancy method with the Sartorius density set. Relative error of the density is dependent on sample density and the readability of the balance.

Figure 8

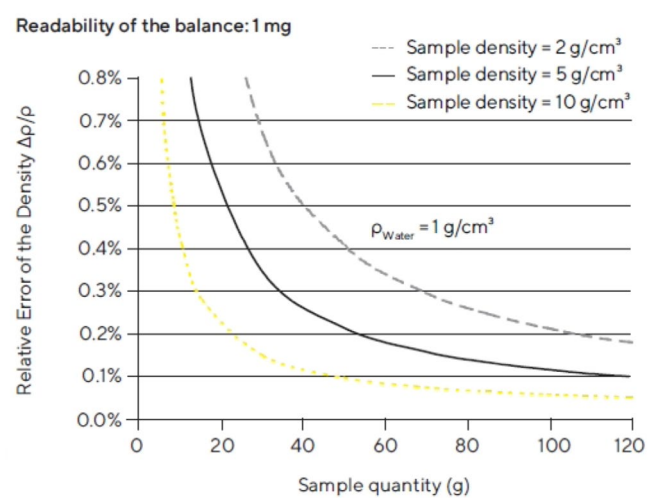


Fig. 8: Relative error of the density during solid density determination by the displacement method. Relative error of the density is dependent on sample size and sample density.

Bulk density measurements of small solid objects using laser confocal microscopy

Adapted from Kilmametov A., *et al.* (2016)

ARTICLE 

Bulk density is defined as weight divided by the volume of a solid and is a fundamental characteristic of matter. It is easily performed on quantities of matter greater than 2 grams with a precision of $\pm 0.005\%$ by using the Archimedean technique: measuring weight in air and measuring volume by displacement in water or other liquid. Density and porosity measurements are used during in-line monitoring of production quality and in powder and mineral technologies.

However, determining the precise density of small samples (≤ 100 mg and especially ≤ 30 mg) presents additional challenges than those of larger samples. Irregularities in the sample may include small fissures, fractures, open pores with access to the surface, and closed or blind pores which are internal in the sample. Irregularities in small samples can increase the difficulty of obtaining precise measurements of density.

Some published examples of density measurements of small samples are listed in Table 1.

The authors presented their refinements of the microscopy-assisted capillary technique to measure the density of small solid objects (e.g., 1 mg) while preserving the precision of assessing the density of larger samples.

Results

The authors used laser confocal microscopy to measure the changes in the meniscus (volume) with accuracy. To avoid the spreading of the liquid outside the Au-coated well after adding the 1 mg sample, the authors coated the outside region around the top of the well with a hydrophobic (CH₃-terminated) self-assembled monolayer and the walls of the well with a self-assembling hydrophilic (COOH-terminated) monolayer (Fig. 1, top panel).

The authors experimented with various surfaces and surface treatments to identify preparations suitable for the measurement of the height of the meniscus. Bare Aluminum and COOH-terminated thiol 11-mercapto-1-undecanol (MUD) 97% (Sigma) did not prevent the spreading of organic liquids (Fig. 1, lower panel). In compari-

son, a micro-contact printing procedure of a 0.2 mmol solution of Octadecylthiol (ODT) in ethanol with additional treatments allowed the test liquids to bead on the surface as indicated by the contact angles. ODT provided a suitable surface for several types of samples. The printing of the hydrophobic and hydrophilic monolayers on their respective surfaces was essential for obtaining reproducible and accurate values of the volume, and thus, the calculated density.

After adding the sample, the meniscus rises in the vertical direction, assuming the well has hydrophilic printed walls. Assuming the footprint of the cap/meniscus and the well match, the change in height of the top or bottom of the cap/meniscus directly determines the added volume. The meniscus often changes from concave to convex. The volume can be calculated with the following formula:

$$V = \pi h(3r^2 + h^2)/6$$

The height h of the meniscus or spherical cap varies in proportion to the size of the added sample(s). The realized contact angle θ value can be estimated when the angle is $\leq 22^\circ$, the radius is $1500 \mu\text{m}$, and the $h/r \leq 0.2$ or $h \leq 285 \mu\text{m}$.

Laser confocal microscopy of the liquid meniscus

A laser scanning confocal microscope can obtain high-resolution optical images with selectivity of depth by using an objective lens to focus a beam through the light source aperture into a small focal volume on the irradiated surface and obtain the height and diameter of the meniscus. The meniscus height was measured with an

Table 1: Previous methods used to measure density of small samples.

30-100 mg	Rise of liquid meniscus in measuring container	±3%	Caley, 1930 https://pubs.acs.org/doi/abs/10.1021/ac50070a014	Microdensitometer and displacement liquid is ethyl ether
30 mg	Optical microscopy measured height of liquid meniscus	±0.5%	L. D. Muller, 1960 Proc. Institute of Mining and Metallurgy, Paper No. 52, London	Optical microscopy improved precision
2 mg	Optical microscopy measured height of liquid meniscus	±1.0%	L. D. Muller, 1960 Proc. Institute of Mining and Metallurgy, Paper No. 52, London	Optical microscopy improved precision

accuracy of $\pm 0.5 \mu\text{m}$. A reference level for the plate surface was obtained by averaging four additional readings focused on the surface around the cavity.

In Figure 2, depth-selected optical images were captured with the scanning protocol and are presented as a single cross-section at a time. The z-sequence of images provides evidence for precise determination of the height of the liquid: Meniscus (trough) or spherical cap (top) corresponds to the highest intensity in the sequence of images.

The sensitivity of the technique is dependent on the magnification of the used objective of the microscope. Using a 10x objective, a well with $r=1500 \mu\text{m}$, a 1 mm^3 sample, and an observed change in height of $5 \mu\text{m}$ (from 100μ to 105μ) provided a difference in volume of $2 \times 10^{-3} \mu\text{L}$. The accuracy of the calculated density is 0.16%. Using a 20x or 40x magnification objective can improve the accuracy of measuring the height of the meniscus and the density determination to $\pm 0.25 \mu\text{m}$ and $\pm 0.08\%$, respectively.

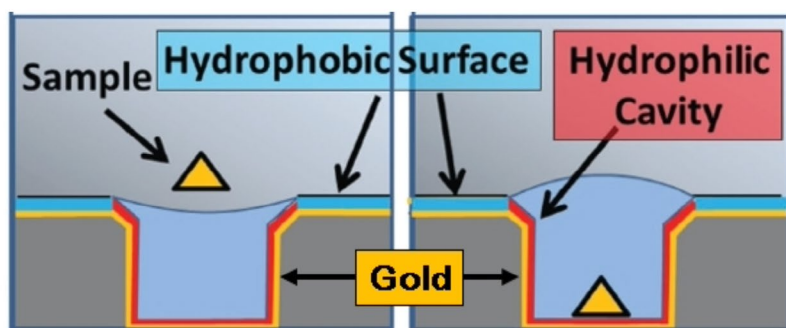
Density measurements

To minimize evaporation, the authors used the liquid dimethyl phthalate (DMP) as the solution in the wells for measuring the volume of the gold (Au), palladium (Pd), or tungsten (W) samples. Before immersion, solid objects were degreased by acetone and may have been subjected to plasma cleaning. Sometimes after sample addition, they adjusted the horizontal position of the cavity to ensure the beam of the laser confocal microscope focused on the meniscus extremum (top or bottom) and captured a series of depth-selective images.

Gold samples

As a reference, high-purity gold (99.9%) has a well-established density ($19,320 \text{ kg/m}^3$).

Figure 1



Static Contact Angles	Dimethylphthalate (DMP)	Water (H ₂ O)	Paraffin Oil
Aluminium	$18^\circ \pm 2^\circ$	$34^\circ \pm 1^\circ$	$7^\circ \pm 3^\circ$
Au MUD-Treated	$10^\circ \pm 2^\circ$	$35^\circ \pm 0,5^\circ$	$15^\circ \pm 1^\circ$
Au (ODT-Printed)	$69^\circ \pm 2^\circ$	$100^\circ \pm 1^\circ$	$46^\circ \pm 1^\circ$

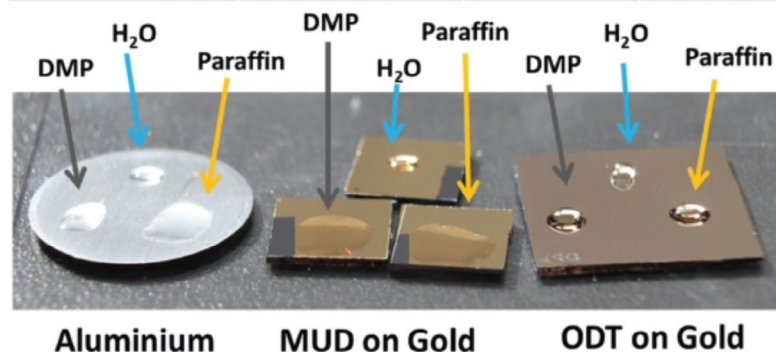


Fig. 1: Preparation of the surfaces for the reproducible measurements of volumes of small samples. (Upper panel) After coating with gold for surface functionalization (gold-colored area), walls and bottom were printed with self-assembling hydrophilic monolayer and boundaries with a self-assembling hydrophobic material. The well was partially filled with dimethyl phthalate (DMP), water, or paraffin oil. (Lower panel) Wetting of the utilized surfaces was characterized by visual assessment and static contact angles. The untreated aluminium and the COOH-terminated thiol 11-mercapto-1-undecanol (MUD) 97% (Sigma) on gold surfaces allowed the test liquids to spread. In contrast, an Octadecylthiol (ODT) printed surface supported a high meniscus for droplets of water, DMT, and paraffin oil.

Figure 2

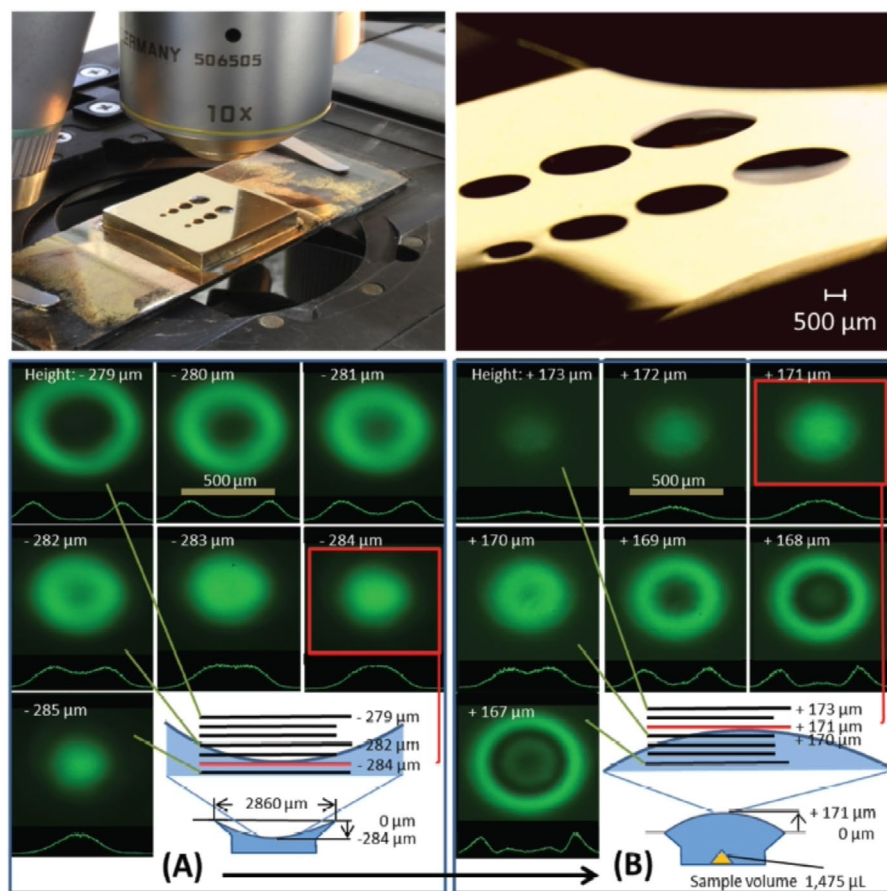


Fig. 2: Measuring the height of the meniscus before and after sample addition by laser confocal microscopy. The shape and height of the liquid meniscus are captured by the z-sequence of images which are a set of cross-sections. (A) Before addition of sample. Meniscus is concave with a focal point at 284 μm . (B) After addition of sample (1.475 μL), the shape of the meniscus changes to convex with a maximal intensity at +171 μm .

Small samples of thin 0.2 mm Au wire were cut into short segments, so each weighed between 1-3 mg. The authors used laser confocal microscopy to accurately measure the height of the meniscus before and after the addition of one or more Au gold wire segments in up to 24 samples. The z-position of the extremum of the meniscus ranged from negative values (concave meniscus) to positive values (convex meniscus). Experimental errors were up to 1% for samples that had changed the shape of the meniscus to a flat surface. The bulk density was derived from the mass of the specimen(s) and the values of the volume by using Formula 1. The slope of the plot of the mass/volume for the 24 samples equals 19.31 g/cm^3 , with an accuracy of 0.05%. The calculated density agrees with the literature and international standards (19,310 kg/m^3 SI units).

The sensitivity of the method was determined with small Au spheres with a

weight of 3-10 mg and a radius ranging from 1.5 to 0.3 mm. However, density calculations from the volume and mass observations of the spheres indicated a lighter density which suggested either a mixture of lighter alloys with the gold or internal porosity. The high purity of the Au samples was confirmed by energy dispersive X-ray. Images of the spheres by a scanning electron microscope revealed a single small shrinkage cavity in each sphere.

Thus, the specimens had excess volume due to a shrinkage cavity. To reduce the effects of shrinkage cavity on volume, the authors treated the mounted cavity plate with immersed samples inside a desiccator with 20 mbar pressure for 5 min. The air bubbles rose to the surface during this time and reduced the height of the meniscus. The evaporation of liquid under these desiccator conditions was measured on a cavity (same radius and liquid height) with no samples: the volume decreased by 0.26 μL .

Calculations of bulk density before desiccation (19.01 g/mL) were lower than after desiccation (19.31 g/mL). The Au density calculation based on desiccated samples showed an accuracy of 0.3% which supports the use of this methodology for samples, even with open pores.

Compressed materials

Powder technology requires the accurate determination of the bulk density of powdered or granular materials. Interparticle space (voids or pores) presents a challenge, and its total volume depends on the following five factors:

- Particle size
- Size distribution of particles
- Degree of compaction
- Degree of sintering (heat treatment that can increase structural integrity and intrinsic strength)

The authors chose palladium (Pd) and tungsten (W) as model systems. The compacted powders (pressures from 200 to 2000 MPa) formed 8 mm pellets and small pieces weighing 1-3 mg were used for density measurements. The samples were measured before and after vacuum treatment, to uncover the contribution of porosity to the volume (Fig. 3). The upper curve for Pd in Figure 3a shows the effect of vacuum treatment on measured density values compared to the lower curve. Open and closed porosity account for the area above the as-received density curve whereas closed porosity explains the area above the upper-density curve to the theoretical density. Closed porosity is absent in the 10 μm Pd powder that had been compressed with 600 MPa.

The W powder has a finer particle size ($\leq 1\mu\text{m}$) with more closed porosity, as indicated by the qualitative characteristics of the density-pressure curves (Fig. 3d). Closed porosity reached 8% to 10% in powders compacted with 400-600 MPa and reached 11% to 12% at higher pressures. Vacuum application was essential for determining the real bulk density of samples, although closed porosity still affected bulk density.

Several parameters influenced the degree of open and closed porosity between the two metals. In addition to the four aforementioned factors, the following characteristics also contributed:

- Different mechanical properties (W is brittle and Pd is ductile with more tensile strength)
- Different melting temperatures
- Different levels of pressure-induced sintering

Organic hydrophobic materials

Bulk density measurements for organic compounds are important in organic and polymer development and production. The authors chose to use amorphous fluoropolymer Teflon AF 1600 DuPont with a bulk density of 1.78 g/mL as an example of an organic hydrophobic material. They compactly twisted the Teflon tape to resemble a spherical shape and unfortunately introduced some open porosity. The second example was a porous membrane (0.1 μm pore size from Whatman). Both solids float on DMP whereas a convenient test liquid for hydrophobic organics is liquid paraffin due to minimal or no detectable evaporation at room temperature, low density (0.82 g/mL), and high wetting ability.

The twisted Teflon samples float on paraffin and degassing causes the release of air bubbles which rise to the surface and may swell the meniscus. After all the air bubbles burst, the Teflon samples sank to the bottom. As aforementioned, the printing of a self-assembling hydrophobic monolayer on the Au platform was essential to prevent overspreading of the paraffilm.

Conclusion

The examples of Au, Pd, and W show the applicability of this technique in measuring the volume of small samples of solid or powdered metals. Preparation of the surface of the well and bordering surfaces with hydrophilic and hydrophobic self-assembling monolayers respectively were essential for reproducible and accurate assessment of the height of the meniscus. Some samples may require vacuum treatment to remove air bubbles due to open porosity. This approach modified by using paraffin oil as the solution is also applicable to hydrophobic porous materials.

Figure 3

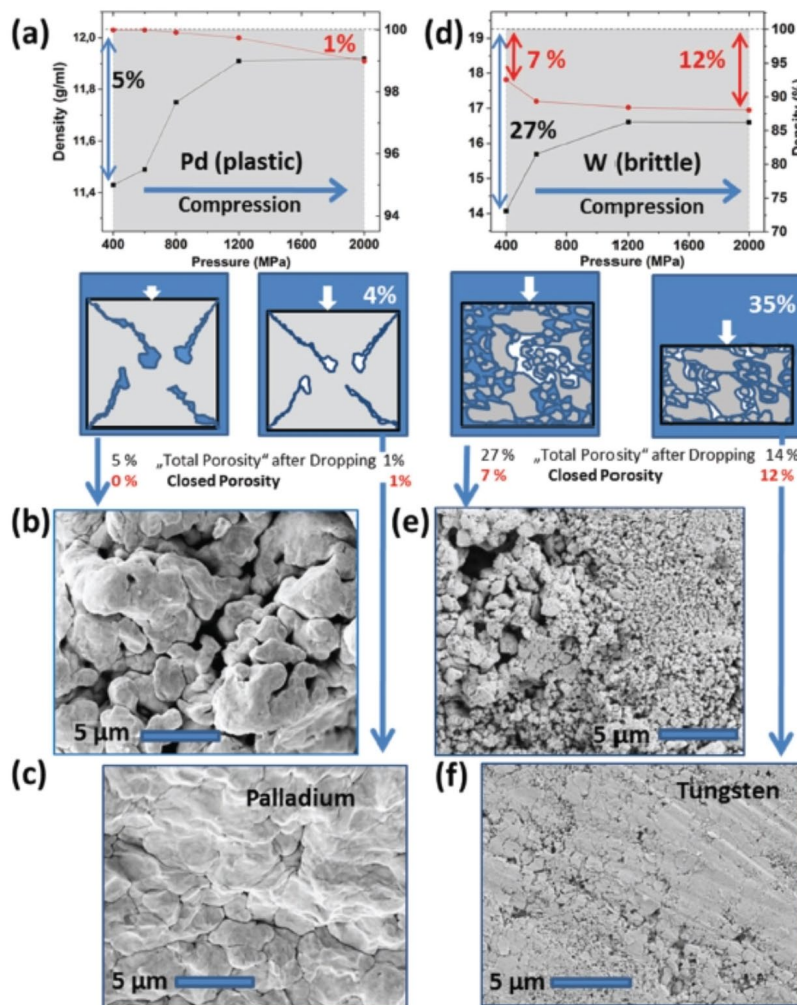


Fig. 3: Measurements of open and closed porosity in powders with different particle sizes under applied pressure during compaction into solid objects. (a-c) Palladium (Pd) powders with pore sizes of 10 μm. (d-f) Tungsten (W) with pore sizes of ≤1 μm. (a, d) The measured sample volumes, before and after vacuum treatment, reveal the amount of total and closed porosity. (b, e) Scanning electron microscope (SEM) images for the two metallic powders at compaction pressures of 400 MPa. The different degrees of densification affect the presence of internal pores and voids. (c, f) Extent of densification under compaction pressure of 2000 MPa for Pd powder (c) and W powder (f).

The mass of the samples was measured using a Sartorius SE2 ultra-microbalance that delivers a capacity of 2.1 g and 0.1 μg accuracy. The microbalance featured the EUREKA air buoyancy correction software, allowing true mass measurement and compensation for fluctuations in air density within 10 s at each weighing operation. [Sartorius SE2 ultra-microbalance](#)

Solid freeform fabrication of porous calcium polyphosphate structures for bone substitute applications: In vivo studies

Adapted from Shanjani Y., et al. (2013)

ARTICLE 

Bone reconstruction may be required due to trauma, disease, or congenital deformity. The ideal bone replacement displays these five characteristics:

- Osteoinductivity
- Osteoconductivity
- Ability to osseointegrate
- Osteogenicity
- Mechanical strength (e.g., resists fracture)

Although autologous bone grafts exhibit these characteristics, the bone volume needed for the repair may not be available when needed. Other bone substitutes

include allografts and several synthetic bone biomaterials.

Allografts can support osseointegration and osteoconductive with surface preparation. However, allografts have a risk of infection.

Several synthetic bone biomaterials are being investigated: the authors prefer calcium polyphosphate (CPP) substitutes because CPP can be biodegradable for complete replacement and bone ingrowth and cartilage anchorage have been accomplished in vivo. CPP can be manufactured

with conventional powder sintering into a variety of forms with the required extent of porosity. Higher compressive strength can be obtained by solid freeform fabrication (SFF) and its mechanical strength appears to be influenced by the orientation of stacked layers. Here the authors investigated the in vivo characteristics of conventionally sintered (CS) CPP with two types of implanted solid freeform fabricated porous CPP bone substitutes in the rabbit femoral condyle sites for 6 weeks: SFF- horizontal orientation (SFF-H) and SFF-V vertical

Figure 1

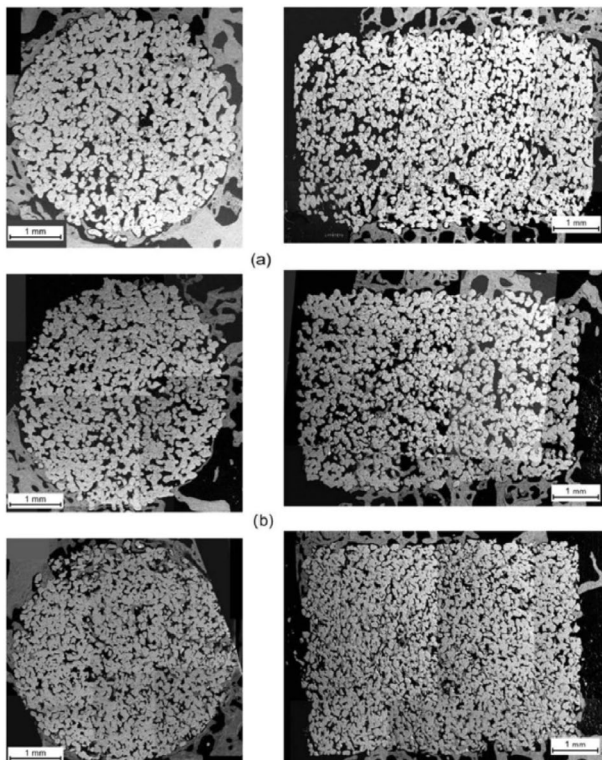


Fig. 1: BS-SEM images of radial (left panels) and longitudinal (right panels) cross-sections (a) SFF-V, (b) SFF-H, and (c) CS implanted samples. The porous CPP implants showed evidence of new bone throughout the 4-mm cross-sectional diameter, and they appeared fixed securely by the bone ingrowth.

Figure 2

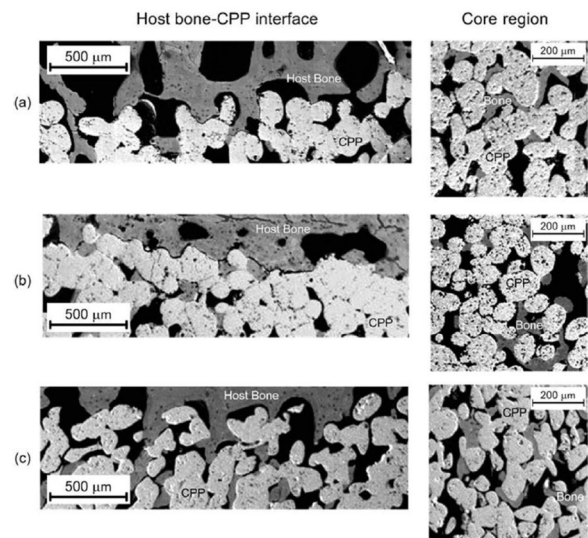


Fig. 2: BS-SEM images show bone formation in two regions of the three types of implants: (a) SFF-V, (b) SFF-H, and (c) CS. (Left panels) Images showing integration of host bone formation into CPP constructs at the interface. (Right panels) Images showing host bone formation in the core region of the implants.

Table 1: Quantitative Effect of Host on implants in different regions: percentage of the void area filled with bone and percentage of degradation.

Percentage of void area filled by formation of host bone					
Implant	Anterior	Posterior	Distal	Proximal	Ave ± SEM
SFF-V	39.01 ± 2.56	33.61 ± 4.44	36.00 ± 3.48	31.44 ± 1.27	35.01 ± 3.25
SFF-H	35.41 ± 3.43	33.58 ± 4.04	31.94 ± 7.67	32.65 ± 7.22	33.39 ± 1.50
CS	35.99 ± 5.91	37.46 ± 13.92	32.70 ± 10.32	39.38 ± 4.78	36.38 ± 2.82
Percentage of degradation of bone in implants					
Implant	Anterior	Posterior	Distal	Proximal	Ave ± SEM
SFF-V	11.72 ± 5.42	10.50 ± 2.12	8.49 ± 6.23	5.59 ± 2.02	9.08 ± 2.67
SFF-H	9.09 ± 8.85	6.92 ± 4.47	10.59 ± 4.35	5.18 ± 6.30	7.94 ± 2.38
CS	9.55 ± 2.04	5.81 ± 1.72	5.60 ± 0.71	8.95 ± 2.05	7.48 ± 2.06

CS, conventionally sintered implant; SFF-H, solid freeform fabrication horizontal orientation; SFF-V, solid freeform fabrication vertical orientation

orientation. The SFF-made bone substitutes were implanted with the orientation of its stacked layers perpendicular to the bone (SFF-H) or implanted in parallel (SFF-V) with the longitudinal bone axis.

The theoretical densities of the CPP implants were measured by the Archimedes technique. The full theoretical density of the three types was similar. The SFF-V, SFF-H, and CS implants had an average density of 72.11 ± 1.35 , 69.69 ± 3.03 , and 70.05 ± 1.24 , respectively.

In vivo assessment

After six weeks, each implant was harvested, fixed in 10% formalin, dehydrated in ethanol followed by xylene, infiltrated with Osteo-Bed resin, and cured. One implant-bone block was sectioned transversely, and the remaining implant-bone blocks were sectioned through the center of the implant and longitudinally and transversely to provide four sections: anterior, posterior, distal, and proximal. A series of graded silicon carbide papers were used to polish all cut surfaces of the samples for both quantitative and qualitative assessment for bone ingrowth and degradation. Quantitative analysis used captured back-scattered scanning electron microscopy (BS-SEM) images, and thin sections of some samples were prepared for histological analysis to visualize the bone ingrowth.

In vivo response

Since no evidence of chronic inflammatory or cytotoxic response appeared in the implants by 6 weeks, the CPP porous

structures appeared to be biocompatible, in agreement with previous reports. Qualitative assessments of BS-SEM images indicated new bone was laid down in the porous CPP implants throughout the 4-mm cross-sectional diameter (Fig. 1, left panels).

Significant bone ingrowth was observed in the different regions of the implants (Fig. 2). The interface between the host bone junction and the implants showed significant bone ingrowth (left panels). Furthermore, the central core regions of the three implants also showed significant bone ingrowth (right panels).

The quantitative data in Table 1 show that the formation of the host bone had filled approximately 30-40% of the available pore area in each of the four regions (anterior, posterior, distal, proximal) of the three types of CPP implants. No significant difference was detected between regions or between types of CPP implants.

Furthermore, the percentage of average degradation of the bone implants ranged from 5-12% in the different regions. The average degradation for all regions in the SFF-V, SFF-H, and CS implants were 9.08 ± 2.67 , 7.94 ± 2.38 , and 7.48 ± 2.06 , respectively. No significant difference was reached among the groups, although the sample size was small. The authors did not mention whether the areas of degradation were adjacent or overlapped with the areas of bone formation.

Histological analysis

Extensive bone ingrowth for the three CPP samples was observed at 6 weeks by histological examination of thin sections from the

Figure 3

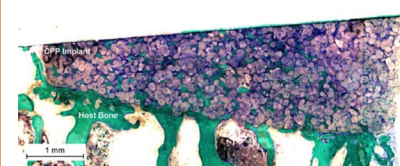


Fig. 3: A representative histological examination of thin sections from the retrieved bone implant blocks at 6 weeks post-implant. The formation of host mineralized bone is shown in green.

retrieved bone implant blocks. The SFF-V, SFF-H, and CS implants showed no evidence of adverse tissue reaction which agrees with previous reports of biocompatibility of these CPP biomaterials. Figure 3 shows a representative histological section (SFF-H) with the mineralized bone shown in green.

Summary

The SFF implants were observed to reach similar levels of host bone infiltration (30-40%) as the CS implants at 6 weeks in rabbits. No significant differences were reached between the SFF-V and SFF-H implants which had different orientations of porosity. Degradation of bone substitutes in implants averaged 7-9%, regardless of regions and types of CPP implants. As an advantage, the SFF method for the preparation of porous CPP implants offers the potential to combine medical imaging with computer-aided design (CAD) to produce custom-made patient-specific implants without requiring extensive post-fabrication machining.

The porosity of each sintered sample was determined using the Archimedes method (ASTM C373) with ethanol as the buoyancy medium (Sartorius YDK01 Density determination Kit). [Sartorius YDK01 Density determination Kit](#)

[BACK TO CONTENTS](#)

Imprint

© Wiley-VCH GmbH
Boschstr. 12,
69469 Weinheim,
Germany
Email: info@wiley-vch.de

Editors
Dr. Martin Graf-Utzmann & Róisín Murtagh

Senior Account Manager:
Jan Käppler

Sartorius Lab Instruments GmbH & Co. Kg
Otto-Brenner-Str. 20,
37079 Goettingen,
Germany